Analytical Prediction of Height-Velocity Diagram of a Helicopter Using Optimal Control Theory

Yoshinori Okuno,* Keiji Kawachi,† and Akira Azuma‡
University of Tokyo, Tokyo, Japan
and
Shigeru Saito§
National Aerospace Laboratory, Tokyo, Japan

The autorotative landing of a single-engine helicopter following power failure is analyzed using optimal control theory. The optimization problems are formulated to minimize the unsafe region in the height-velocity diagram under the condition that the touchdown speed is within the capability of the landing gear. Nonlinear equations of motion are described using a rigid-body dynamic model with longitudinal three degrees of freedom. The aerodynamic model of the rotor takes account of the effects of blade stall during descent and increased induced flow in the vortex ring state. The present method gives a good estimation of the height-velocity boundary in comparison with the existing flight test data. It is pointed out that the test pilot started the collective flare earlier than that occurred in the optimal solution.

Nomenclature

a = lift-curve-slope of blade section, = 5.73
b = number of blades
C_D, C_L = drag and lift coefficients of wing or fuselage
C_d, C_l = drag and lift coefficients of blade section
C_{d0} = profile drag coefficient of blade section
C_H = H-force coefficient = $H/\rho SR^2\Omega^2$, see Fig. 3
C_{M_Y} = hub moment coefficient = $M_Y/\rho SR^3\Omega^2$
C_Q = torque coefficient = $Q/\rho SR^3\Omega^2$
C_T = thrust coefficient = $T/\rho SR^2\Omega^2$, see Fig. 3
c = blade chord
h = distance above c.g., see Fig. 3
I = moment of inertia
i_s = inclination of rotor shaft, positive forward
k_f = $k_\beta/m_\beta R^2\Omega^2$
k_β = spring constant of flapping hinge
l = distance behind c.g., see Fig. 3
m = mass
n = vertical load factor
R = rotor radius
S = rotor disk area, = πR^2
t = time from power failure
v = induced velocity, nondimensionalized by $R\Omega$
x = radial location of blade element, = r/R
$\overline{x_\beta}$ = $\int_{r_\beta}^{R} r(\mathrm{d}m_\beta/\mathrm{d}r)\,\mathrm{d}r/m_\beta R$
α = angle of attack
α_e = effective angle of attack of blade section at $0.75R$, defined by Eq. (22c)
γ = flight-path angle, positive climbing, or Lock number, = $\rho acR^4/I_\beta$
θ_s = longitudinal cyclic pitch, positive nose up
θ_t = blade twist angle, positive twist up
θ_0 = collective pitch at $0.75R$
λ = inflow ratio, Eq. (13)
μ = advance ratio, Eq. (12)
ν = descent ratio, Eq. (12)
$\bar{\nu}$ = $bm_\beta/\rho SR$
ρ = air density
σ = rotor solidity = $bc/\pi R$

Subscripts

a = slack variable
B = relative to body-fixed axes
F = fuselage
f = time of touchdown
H = horizontal stabilizer
R = rotor
stall = after stall
β = flapping hinge

Received Feb. 13, 1989; revision received Dec. 18, 1989.

*Graduate Student, Department of Aeronautics; currently Researcher at National Aerospace Laboratory, Tokyo, Japan.
†Associate Professor, Department of Aeronautics. Member AIAA.
‡Professor Emeritus. Member AIAA.
§Senior Researcher. Member AIAA.

Introduction

HELICOPTERS have a chance of surviving the effects of power failure by using an autorotative descent and landing as illustrated in Fig. 1. Success of the landing depends on various factors such as the ambient conditions, the gross weight, and the skill of the pilot. Unsafe conditions are illustrated in terms of height and velocity as shown in Fig. 2. Usually flight tests are conducted to verify safety in case of power failure. These tests, however, involve significant cost and time due to high risk. These problems have clearly defined the need for methods of predicting unsafe flight conditions and of improving safety in case of power failure.

In response to this need, optimal control theory has been applied to the autorotative flight of helicopters. Komoda[1]

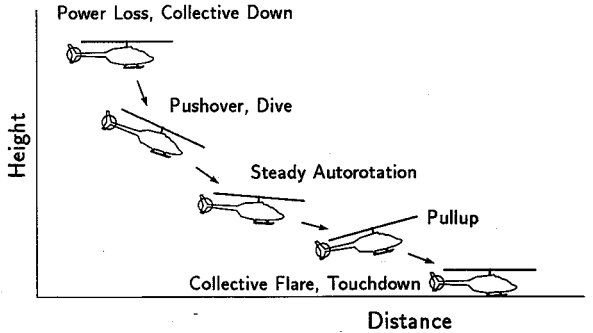

Fig. 1 Autorotative descent and landing following power failure.

solved the optimization problems to minimize or maximize the height difference during maneuver for the specified touchdown conditions. He used linearized equations of motion of a point-mass dynamic model. Johnson[2] used nonlinear optimal control theory to obtain the control procedure required to minimize a weighted sum of the squares of vertical and horizontal velocities at touchdown for the given initial flight conditions. Lee et al.[3] extended this work using a numerical solution technique that can handle the problems with state-variable inequality constraints. In Ref. 4, the authors applied a similar optimization technique to a rigid-body dynamic model combined with the aerodynamic model that was verified experimentally. In this paper, this method has been extended to predict the height-velocity (H-V) boundary explicitly. The repetitive application of the optimization procedure with performance indices involving height and velocity variables allows the minimization of the H-V boundary.

Dynamic Model of the Helicopter

The motion of the helicopter is expressed by using a rigid-body dynamic model with longitudinal three degrees of freedom as shown in Fig. 3. The state variables are height loss z, horizontal velocity u, rate of descent w, pitch attitude Θ, pitch rate q, and rotor rotational speed Ω. The control variables are collective pitch θ_0 and longitudinal cyclic pitch θ_s. The equations of motion relative to the axes fixed in space are described as follows:

$$\frac{dz}{dt} = w \tag{1a}$$

$$\frac{du}{dt} = -\frac{1}{m}(T_B \sin\Theta + H_B \cos\Theta + D_F \cos\alpha_F) \tag{1b}$$

$$\frac{dw}{dt} = -\frac{1}{m}(T_B \cos\Theta - H_B \sin\Theta + D_F \sin\alpha_F) + g \tag{1c}$$

$$\frac{d\Theta}{dt} = q \tag{1d}$$

$$\frac{dq}{dt} = \frac{1}{I_{B_Y}}(M_Y - T_B \cdot l_R + H_B \cdot h_R - L_H \cos(\Theta - \gamma) \cdot l_H) \tag{1e}$$

$$\frac{d\Omega}{dt} = -\frac{1}{I_R} Q \tag{1f}$$

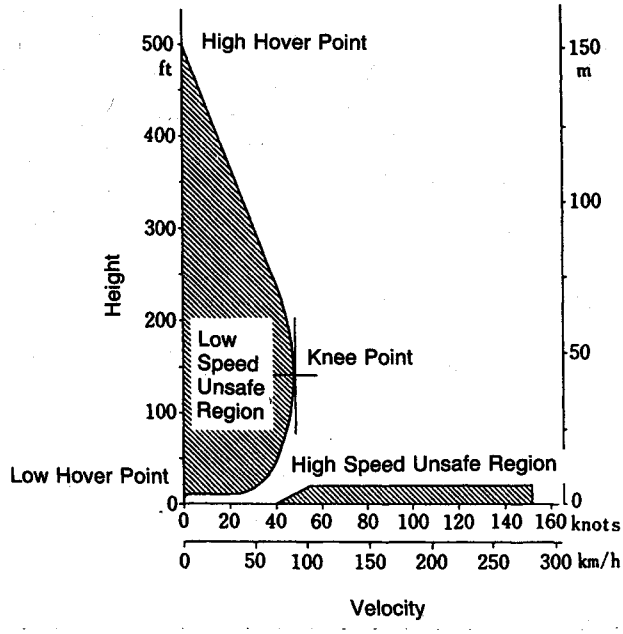

Fig. 2 Typical height-velocity diagram.

where

$$\begin{pmatrix} T_B \\ H_B \end{pmatrix} = \begin{pmatrix} \cos i_s & \sin i_s \\ -\sin i_s & \cos i_s \end{pmatrix} \begin{pmatrix} T \\ H \end{pmatrix} \tag{2}$$

The lift of the horizontal stabilizer L_H is given by

$$L_H = \frac{1}{2}\rho(u^2 + w^2) S_H C_{L_H} \tag{3a}$$

$$C_{L_H} = \begin{cases} a_H \alpha_H & \text{if } \alpha_H \le \alpha_{\text{stall},H} \\ a_H \alpha_{\text{stall},H} & \text{otherwise} \end{cases} \tag{3b}$$

$$\alpha_H = \Theta + i_H + \tan^{-1}\{(w + l_H \cdot q)/u\} \tag{3c}$$

The horizontal and the vertical components of the drag of the fuselage are assumed to be given by

$$D_F \cos\alpha_F \simeq \frac{1}{2}\rho u^2 S_F C_{D_F} \tag{4a}$$

$$D_F \sin\alpha_F \simeq 0 \tag{4b}$$

Rotor Performance in Autorotation

Helicopters encounter an unsteady flow condition known as the vortex ring state when power fails in hover. In the vortex ring state, the slipstream does not develop infinitely. Therefore, momentum theory cannot be applied theoretically to the rotor performance in the case of power failure. In the present study, an empirical model of the induced flow is developed as follows:

$$\frac{v}{\bar{v}} = \left(\frac{v}{\bar{v}}\right)^{C_1} \sin^2\alpha_R \pm \sin\alpha_R \cdot \sqrt{\left(\frac{\bar{v}}{v}\right)^2 - \left(\frac{v}{\bar{v}}\right)^2 (C_2 \sin^2\alpha_R + \cos^2\alpha_R)} \tag{5}$$

where

$$\bar{v} = \sqrt{C_T/2} \tag{6}$$

$$\alpha_R = \tan^{-1}(v/\mu) \tag{7}$$

C_1 and C_2 are empirical constants, which are determined to give the mean values of the scattered experimental data[5] as shown in Fig. 4:

$$C_1 = 1/2, \qquad C_2 = (1 + \sqrt{2})^{-4} \tag{8}$$

When $C_1 = 1$ and $C_2 = 0$, Eq. (5) equals the simple momentum equation. When the nondimensional rate of descent $v/\bar{v}$ is greater than 2 (i.e., in the windmill state) or the rotor angle of attack is not large ($\alpha_R \ll 90$ deg), the effects of the coefficients C_1 and C_2 become small and Eq. (5) nearly equals the simple momentum equation.

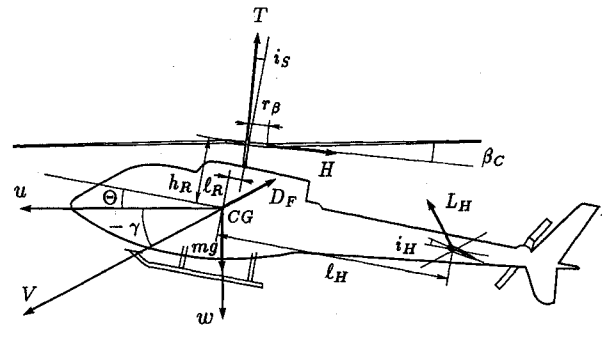

Fig. 3 Helicopter model.

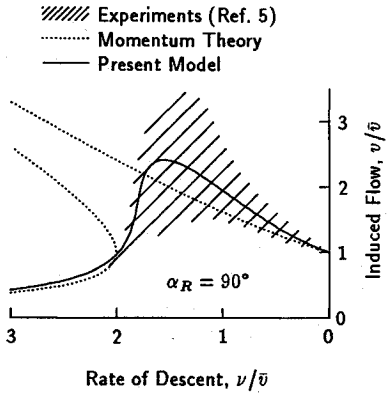

Fig. 4 Induced-flow variation with rate of descent.

Thrust, H-force, torque, and longitudinal hub-moment coefficients of the main rotor are calculated by using a modified blade-element theory that accounts for the effects of blade stall near the blade root during descent. The analytical solutions are obtained in the following forms:

$$C_T = \frac{1}{2}a\sigma\left[\frac{B^3 - kx_s^3}{3}\theta_0 - \frac{B^2 - kx_s^2}{2}\lambda + \frac{B^2 - kx_s^2}{2}\mu\theta_s\right] \quad (9a)$$

$$C_H = \frac{1}{4}\sigma\{(1-x_s^4)C_{d0} + x_s^4 C_{d\text{stall}}\}\mu + \frac{1}{2}a\sigma\left[\left\{\frac{B^2 - kx_s^2}{4}\theta_s + \frac{B - kx_s}{2}\mu\theta_0\right\}\lambda + \left\{-\frac{B^3 - kx_s^3}{3}\theta_0 + \frac{3(B^2 - kx_s^2)}{4}\lambda - \frac{B^2 - kx_s^2}{4}\mu\theta_s + \frac{B^2 - kx_s^2}{4}\mu\beta_c\right\}\beta_c\right] \quad (9b)$$

$$C_Q = \frac{1}{8}\sigma\{(1-x_s^4)C_{d0} + x_s^4 C_{d\text{stall}}\} + \frac{1}{2}a\sigma\left[\left\{\frac{B^3 - kx_s^3}{3}\theta_0 - \frac{B^2 - kx_s^2}{2}\lambda + \frac{B^2 - kx_s^2}{4}\mu\theta_s\right\}\lambda + \left\{-\frac{B^4 - kx_s^4}{8}\theta_s - \frac{B^2 - kx_s^2}{2}\mu\lambda - \frac{B^4 - kx_s^4}{8}\beta_c\right\}\beta_c\right] \quad (9c)$$

$$C_{M_Y} = -x_\beta\frac{1}{2}a\sigma\left[\frac{B^3 - kx_s^3}{6}\cdot\frac{q}{\Omega}\right] - \frac{1}{2}x_\beta\bar{x}_\beta\bar{v}\beta_c - \frac{1}{2}\bar{v}k_f\beta_c \quad (9d)$$

where B is the constant tip loss factor, $B = 0.97$.

x_s is the average radius of the blade stall region, which is defined by

$$x_s = \frac{1}{-2\theta_t}\left[\sqrt{\left\{\alpha_{\text{stall}} - \left(\theta_0 - \frac{3}{4}\theta_t\right)\right\}^2 + 4\theta_t\lambda} - \left\{\alpha_{\text{stall}} - \left(\theta_0 - \frac{3}{4}\theta_t\right)\right\}\right] \quad (10)$$

where $\alpha_{\text{stall}} = 12$ deg in this study.

The lift curve of blade section is assumed to be as shown in Fig. 5. Then k is given by

$$k = 1 - C_{l_{\text{stall}}}/C_{l_{\max}} \quad (11)$$

where $k = 0.5$ in this study.

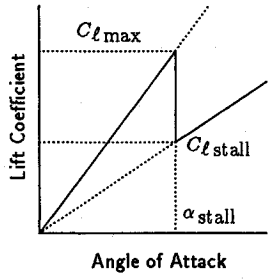

Fig. 5 Lift curve of blade section.

Advance ratio μ, descent ratio v, and inflow ratio λ are given by

$$\begin{pmatrix}\mu\\ v\end{pmatrix} = \begin{pmatrix}\cos(\Theta - i_s - \beta_c) & -\sin(\Theta - i_s - \beta_c)\\ \sin(\Theta - i_s - \beta_c) & \cos(\Theta - i_s - \beta_c)\end{pmatrix} \times \begin{pmatrix}u - h_R\cdot q\\ w + l_R\cdot q\end{pmatrix}/R\Omega \quad (12)$$

$$\lambda = -v + v \quad (13)$$

The longitudinal tilt angle of the tip-path plane β_c is obtained, assuming quasisteady flapping motion, in the following form[6]:

$$\beta_c = \frac{K_{\dot\beta}}{K_{\dot\beta}^2 + K_\beta^2}\left\{-K_1\theta_s - 2K_2\mu\theta_0 + K_3\mu\lambda + (2 + K_\beta)\cdot\frac{q}{\Omega}\right\} \quad (14)$$

where

$$K_\beta = \frac{k_\beta}{I_\beta\Omega^2} + \frac{x_\beta(\bar{x}_\beta - x_\beta)}{I_\beta/m_\beta R^2}, \quad K_{\dot\beta} = \frac{\gamma}{2}\left(\frac{1}{4}B^4 - \frac{2}{3}B^3x_\beta\right)$$
$$K_1 = \frac{\gamma}{2}\left(\frac{B^4}{4} - \frac{B^3}{3}x_\beta\right), \quad K_2 = \frac{\gamma}{2}\left(\frac{B^3}{3} - \frac{B^2}{2}x_\beta\right) \quad (15)$$
$$K_3 = \frac{\gamma}{2}\left(\frac{B^2}{2} - Bx_\beta\right)$$

To show the validity of the present aerodynamic model, measured and calculated variations of the torque coefficient required to generate a constant thrust during vertical descent are compared in Fig. 6. The result of the present model shows better agreement with the experimental data[7] over the entire flight condition from hover to the windmill state than the simple model, in which account is taken neither of the increased induced flow in the vortex ring state, i.e., $C_1 = 1$ and $C_2 = 0$ in Eq. (5), nor of the effects of the blade stall, i.e., $x_s = 0$ in Eqs. (9a–9d).

Formulation of the Optimal Control Problems

Two different optimization problems are formulated. One is the prediction of the H-V boundary. It is based on minimizing the unsafe region under the condition that the touchdown speed is within the capability of the landing gear. The other problem is to find the optimal landing procedure for a given initial flight condition. It is based on minimizing the touchdown speed.

Performance Index and Boundary Conditions

The boundary of the low-speed unsafe region is estimated by calculating three representative points (see Fig. 2): 1) high hover point (point of minimum height), 2) low hover point (point of maximum height), and 3) knee point (point of critical height and minimum velocity). The performance index

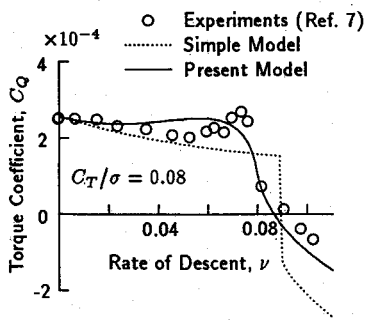

Fig. 6 Necessary torque for a constant thrust in vertical descent.

and the boundary conditions to obtain each point are formulated as follows:

Performance Index

For the high hover point:

$$I = \min z(t_f) \tag{16a}$$

For the low hover point:

$$I = \max z(t_f) \tag{16b}$$

For the knee point:

$$I = \max_{z(t_f)} \{\min u(0)\} \tag{16c}$$

Initial Conditions

For the high hover point and the low hover point,

$$z(0) = 0, \quad u(0) = 0, \quad w(0) = 0, \quad q(0) = 0$$
$$\Theta(0), \quad \Omega(0) \quad \text{given} \tag{17a}$$

For the knee point:

$$z(0) = 0, \quad q(0) = 0$$
$$w(0), \quad \Theta(0), \quad \Omega(0) \quad \text{given} \tag{17b}$$
$$u(0) \quad \text{free}$$

Terminal Conditions

$$\Theta(t_f) = 0, \quad \left(\frac{u(t_f)}{u_s}\right)^2 + \left(\frac{w(t_f)}{w_s}\right)^2 = 1$$
$$z(t_f), \quad q(t_f), \quad \Omega(t_f), \quad t_f \quad \text{free} \tag{18}$$

where u_s and w_s are the horizontal and the vertical components of the maximum allowable touchdown speed.

The performance index and the boundary conditions to find the optimal landing procedure for a given initial flight condition are formulated as follows:

Performance Index

$$I = \min\left\{\left(\frac{u(t_f)}{u_s}\right)^2 + \left(\frac{w(t_f)}{w_s}\right)^2\right\} \tag{19}$$

Initial Conditions

$$z(0) = 0, \quad q(0) = 0$$
$$u(0), \quad w(0), \quad \Theta(0), \quad \Omega(0) \quad \text{given} \tag{20}$$

Terminal Conditions

$$\Theta(t_f) = 0, \quad z(t_f) \quad \text{given}$$
$$u(t_f), \quad w(t_f), \quad q(t_f), \quad \Omega(t_f), \quad t_f \quad \text{free} \tag{21}$$

Table 1 Specifications of the exemplified helicopter

Gross weight, W	5900 kgf
Rotor radius, R	8.534 m
Blade chord, c	0.381 m
Number of blades, b	4
Rotor rotational speed, Ω	239 rpm
Rotor moment of inertia, I_R	7107 kg-m^2
Location of c.g., l_R	0.0254 m

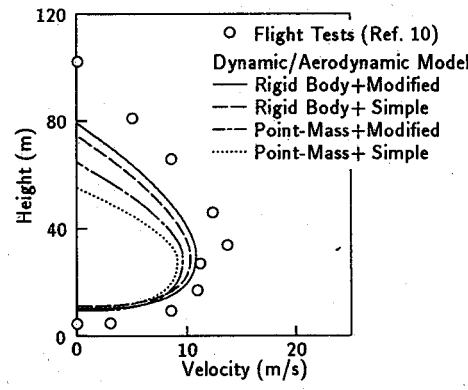

Fig. 7 Effect of dynamic and aerodynamic models on H-V boundary prediction.

Constraints

The following constraints are taken into consideration: 1) the range of collective pitch, 2) the range of cyclic pitch, 3) the maximum value of the effective angle of attack of the blade section at $0.75R$, 4) the maximum value of the vertical load factor, 5) the range of pitch attitude, and 6) the range of rotor speed. These constraints are formulated as follows:

$$\theta_{0_{\min}} \le \theta_0 \le \theta_{0_{\max}} \tag{22a}$$

$$\theta_{s_{\min}} \le \theta_s \le \theta_{s_{\max}} \tag{22b}$$

$$\alpha_e \equiv \theta_0 - \frac{4}{3}\lambda \le \alpha_{\max} \tag{22c}$$

$$\frac{dw}{dt} \ge g(1 - n_{\max}) \tag{22d}$$

$$\Theta_{\min} \le \Theta \le \Theta_{\max} \tag{22e}$$

$$\Omega_{\min} \le \Omega \le \Omega_{\max} \tag{22f}$$

Actually, Eq. (22f) is found unnecessary because no optimal solution violates this constraint in this study. This is because violation of the upper and/or the lower limits of the rotor speed causes an unallowable load factor and/or excessive blade stall, respectively.

The preceding inequality constraints are transformed into equality constraints by introducing "slack variables."[8] Then the state vector $\boldsymbol{x}$ and the control vector $\boldsymbol{u}$ become

$$\boldsymbol{x} = (z,u,w,\Theta,q,\Omega,\Theta_a,\dot{\Theta}_a)^T \tag{23a}$$

$$\boldsymbol{u} = (\theta_0,\theta_s,\theta_{0_a},\theta_{s_a},\alpha_a,n_a,\ddot{\Theta}_a)^T \tag{23b}$$

where Θ_a and $\dot{\Theta}_a$ are slack state variables that are introduced because Eq. (22e) is a second-order state variable constraint, and θ_{0_a}, θ_{s_a}, α_a, n_a, and $\ddot{\Theta}_a$ are slack control variables. Numerical solutions of the nonlinear optimal control problems are obtained through the use of sequential conjugate gradient restoration algorithm developed by Miele et al.[9]

Results and Discussion

The low-speed unsafe region is analyzed for a single-engine helicopter, the specifications of which are listed in Table 1.

The high-speed unsafe region does not exist theoretically because this helicopter has a wheel-type landing gear and the forward speed at touchdown is allowed to be large ($u_s = 30$ mph and $w_s = 8$ fps). The optimal control is started 0.5 s after power failure in order to simulate the initial reaction delay of the pilot.

Prediction of the H-V Boundary

Figure 7 compares the predictions of the low-speed unsafe region for four combinations of the dynamic and the aerodynamic models with flight test data.[10] The combination of the rigid-body dynamic model and the modified aerodynamic model (present theory) provides results that are in closest agreement with the flight test results, particularly in the vicinity of the knee point. The point-mass dynamic model has the merits of simple formulation and short computation time but produces less satisfactory results.

Figure 8 shows the effect of the initial flight-path angle on the size of the predicted unsafe region. The height of the knee point is decreased by increases in the initial flight-path angle because the initial climb rate offsets the height loss after power failure. The velocity of the knee point is higher when the helicopter is climbing rather than descending at the instant of power failure, because the power requirement is higher and the decay of rotor speed is more rapid.

Figure 9 shows the loci of the optimal landing paths from three representative points in the H-V diagram in terms of height, horizontal velocity, and rate of descent. Each path starts from the boundary of the unsafe region determined theoretically and terminates with the maximum allowable touchdown speed. It can be observed that the pilot is required to cope with a high rate of descent and a steep approach, especially in the case of the high hover point. The control histories for the high hover point and the knee point are discussed below. Note that the results of the present theory shown in the following sections are the optimal solutions, not for minimizing the unsafe region but for minimizing the touchdown speed from the initial flight conditions of the flight tests.

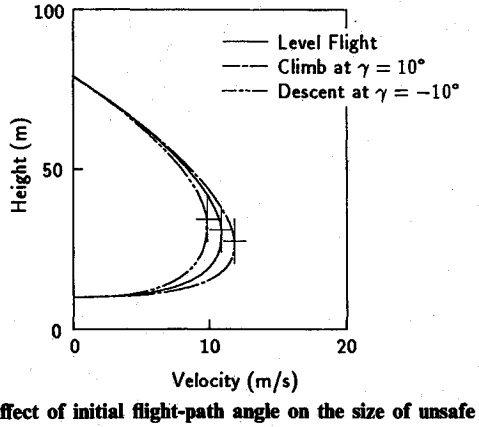

Fig. 8 Effect of initial flight-path angle on the size of unsafe region.

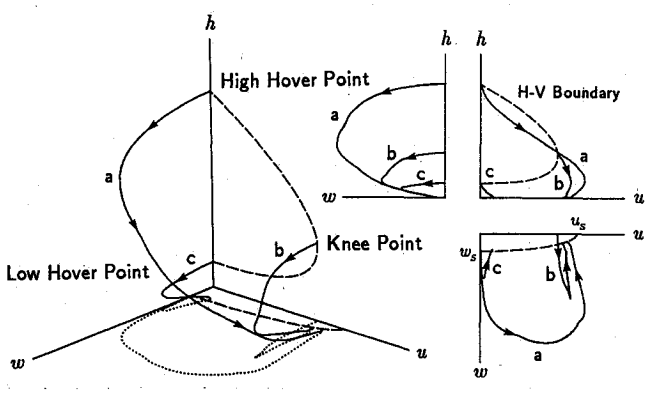

Fig. 9 Loci of optimal landing paths in (h,u,w) space.

Landing from the High Hover Point

Figure 10 compares the time histories of the optimal solutions using two different dynamic models with those from a flight test,[10] for landing from the high hover point. The pitch-attitude history of the optimal solution using the rigid-body model is in good agreement with the flight test data. When the point-mass model is used, however, the optimal solution of pitching motion is of the bang-bang type, which reduces the agreement in the H-V boundary prediction as discussed above.

In the collective pitch histories of Fig. 10, it can be observed that the pilot started the collective flare earlier than that occurred in the optimal solution. This difference is believed to be the reason that the present theory predicts the high hover point to be lower than that measured (see Fig. 7).

Figure 11 shows the effect of the difference in the collective control use during the flare on the touchdown speed. The nonoptimal path is calculated by using the present model for the collective pitch history of the flight test data. It can be observed that the premature collective flare results in a harder landing because of the loss of the rotor rotational energy.

Time histories of the optimal solution are presented in Fig. 12 to show how the amplitude of collective pitch is determined during the collective flare. It can be observed that the collective-pitch angle is limited by the maximum load factor

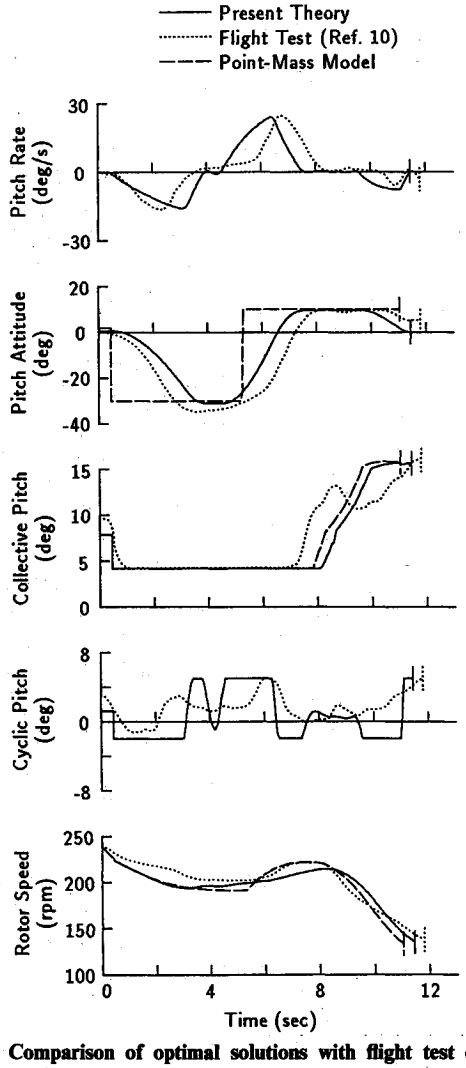

Fig. 10 Comparison of optimal solutions with flight test data[10] for high hover point.

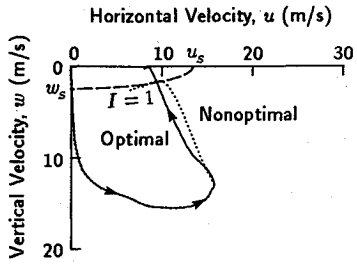

Fig. 11 Comparison of optimal and nonoptimal landing paths from the high hover point.

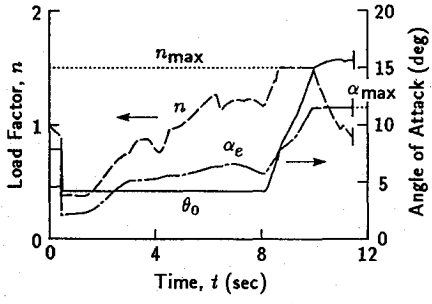

Fig. 12 Time histories of the optimal solution for the high hover point.

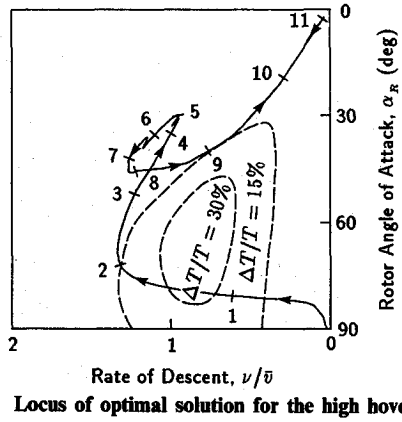

Fig. 13 Locus of optimal solution for the high hover point.

for the earlier period and by the blade stall angle of attack for the later period.

Figure 13 shows the locus of the optimal solution in terms of the rotor angle of attack and rate of descent. The broken lines indicate the severity of thrust fluctuation in the vortex ring state.[5] The numerals indicate the time from the power failure in seconds. It can be observed that the helicopter is in the vortex ring state for the initial two seconds. Through this period, the collective pitch is reduced to the minimum limit and the cyclic pitch is held constant as shown in Fig. 10. Therefore, it is considered that there would be no difficulty of control.

Landing from the Knee Point

Figure 14 compares the time histories of the optimal solution with the flight test data,[10] for landing from the knee point. The difference between the measured and the calculated collective flare is not as significant as observed in Fig. 10. This may be because the approach is not as steep as in the case of the high hover point (see Fig. 9) and the pilot can start the collective flare in the proximity of the ground as occurred in the optimal solution.

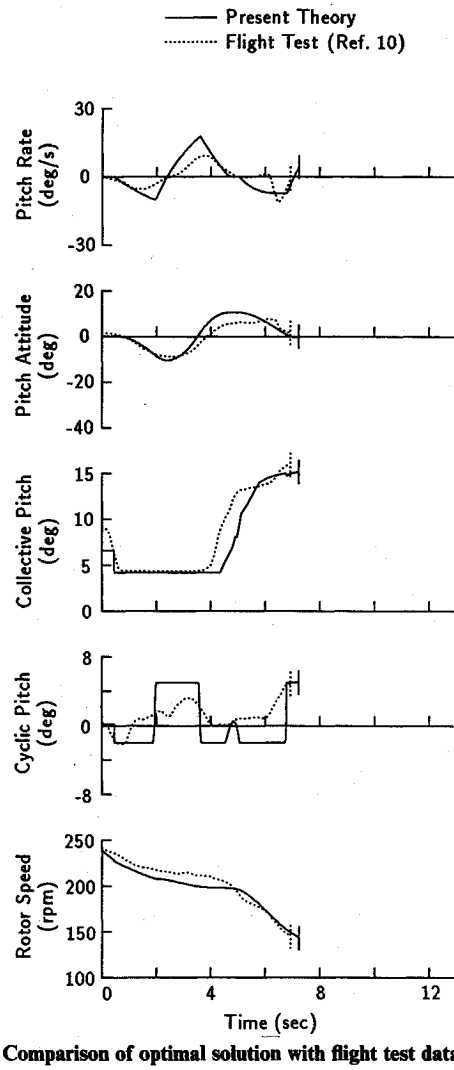

Fig. 14 Comparison of optimal solution with flight test data[10] for knee point.

Conclusions

Nonlinear optimal control theory has been applied successfully to the H-V boundary prediction of a single-engine helicopter. The analytical method proposed in this paper is useful in reducing the risk, cost, and time of flight tests for certification. It presents, as well, the possibility of extending the H-V boundary determined experimentally.

The following conclusions are also drawn:

1) The present theory, which includes the rigid-body dynamic model and the modified aerodynamic model, provides a reasonable prediction of the H-V boundary.

2) The test pilot started the collective flare earlier than that occurred in the optimal solution, especially in the case of landing from the high hover point.

3) The knee point has a higher velocity and a lower height when the helicopter is climbing rather than descending.

References

[1]Komoda, M., "An Analytic Method to Predict Ideal H-V Boundary and CDP of Rotocraft with Special Attention to the Application of Optimizing Techniques," *Joint Symposium on Environmental Effects on VTOL Designs*, American Helicopter Society, New York, Nov. 1970, Preprint SW-70-13; also *Transactions of the Japan Society for Aeronautical and Space Sciences*, Vol. 15, No. 30, 1973, pp. 208–228.

[2]Johnson, W., "Helicopter Optimal Descent and Landing After Power Loss," NASA TM-73244, 1977.

[3]Lee, A. Y., Bryson, A. E., Jr., and Hindson, W. S., "Optimal Landing of a Helicopter in Autorotation," AIAA Paper 86-2287,

1986; also *Journal of Guidance, Control, and Dynamics*, Vol. 11, No. 1, 1988, pp. 7–12.

[4]Okuno, Y., Kawachi, K., Azuma, A., and Saito, S., "Analytical Study of Dynamic Response of Helicopter in Autorotative Flight," *Proceedings of the 14th European Rotocraft Forum*, Italy, Sept. 1988, Paper 71.

[5]Washizu, K., Azuma, A., Koo, J., and Oka, T., "Experiments on a Model Helicopter Rotor Operating in the Vortex Ring State," *Journal of Aircraft*, Vol. 3, No. 3, 1966, pp. 225–230.

[6]Azuma, A., "Dynamic Analysis of the Rigid Rotor System," *Journal of Aircraft*, Vol. 4, No. 3, 1967, pp. 203–209.

[7]Castles, W., Jr., and Gray, R. B., "Empirical Relation Between Induced Velocity, Thrust, and Rate of Descent of a Helicopter Rotor as Determined by Wind-Tunnel Tests on Four Model Rotors," NACA TN-2474, 1951.

[8]Jacobson, D. H., and Lele, M. M., "A Transformation Technique for Optimal Control Problems with a State-Variable Inequality Constraint," *IEEE Transactions on Automatic Control*, Vol. AC-14, No. 5, 1969, pp. 457–464.

[9]Wu, A. K., and Miele, A., "Sequential Conjugate Gradient Restoration Algorithm for Optimal Control Problems with Nondifferential Constraints and General Boundary Conditions, Pt. 1," *Optimal Control Applications and Methods*, Vol. 1, 1980, pp. 69–88.

[10]Hanley, W. J., DeVore, G., and Martin, S., "An Evaluation of the Height-Velocity Diagram of a Heavy-Weight, High Rotor Inertia, Single-Engine Helicopter," Federal Aviation Administration, FAA-ADS-84, 1966.